Dynamic Response and Stability Margin Improvement of Wireless Power Receiver Systems via Right-Half-Plane Zero Elimination

Kerui Li, *Student Member, IEEE*, Siew-Chong Tan, *Senior Member, IEEE*, and Shu Yuen Ron Hui, *Fellow, IEEE*

***Abstract*—The series-series compensation topology is widely adopted in many wireless power transfer applications. For such systems, their wireless power receiver part typically involves a dc–dc converter with front-stage full-bridge diode rectifier, to process the high-frequency transmitted ac power into a dc output voltage for the load. It is recently reported that the current source nature of the series-series compensation will introduce right-half-plane (RHP) zeros into the small-signal transfer functions of the dc–dc converter of the wireless power receiver, which will severely affect the stability and dynamic response of the system. To resolve this issue, in this article, it is proposed to adopt a different rectifier configuration for the system such that the input current to the dc–dc converter becomes controllable to eliminate the presence of RHP zeros of the small-signal transfer functions of the system. This rectifier can be applied to different wireless power receivers using the buck, buck-boost, or boost converters. As compared with the original wireless power receivers, the modified ones feature minimum-phase characteristics and hence ease the design of compensator. Theoretical and experimental results are provided. The comparative experimental results verify the elimination of the RHP zero, improved dynamic responses of reference tracking and against load disturbances, and a larger stability margin.**

***Index Terms*—Dynamic response, right-half-plane zero (RHP), stability, wireless power receiver, wireless power transfer.**

I. Introduction

THE WIRELESS power receivers which comprise a front-end diode rectifier and a post dc–dc converter [1], [2], are popular solutions for wireless charging applications. Since the rectified dc voltage provided by the diode rectifier does not necessarily match the voltage requirement of the load, the dc–dc converters are hence utilized to match the voltage difference and regulate the output voltage [1], [3].

Manuscript received November 27, 2020; revised February 25, 2021; accepted April 9, 2021. Date of publication April 20, 2021; date of current version June 30, 2021. Recommended for publication by Associate Editor R. Zane. *(Corresponding author: Kerui Li.)*

Kerui Li and Siew-Chong Tan are with the Department of Electrical and Electronic Engineering, The University of Hong Kong, Hong Kong (e-mail: krli@connect.hku.hk; sctan@eee.hku.hk).

Shu Yuen Ron Hui is with the School of Electrical and Electronic Engineering, Nanyang Technological University, Singapore 639798, Singapore, and also with the Department of Electrical and Electronic Engineering, the Imperial College London, SW7 2AZ London, U.K (e-mail: ron.hui@ntu.edu.sg).

Color versions of one or more figures in this article are available at https://doi.org/10.1109/TPEL.2021.3074324.

Digital Object Identifier 10.1109/TPEL.2021.3074324

The charging profile of the battery imposes strict requirements on the charging current and voltage [4], which, in turn, raises new challenges on the output voltage/current regulation of the wireless power receivers [5], [6]. Despite many research efforts on improving the regulation capability of the dc–dc converters, these works are not necessarily applicable to those dc–dc converters used in wireless power receivers. Conventional dc–dc converters are designed under the condition of voltage source input. However, the input of the dc–dc converters employed in wireless power receivers is of current source nature when adopting the series-series compensation [7], [8]. This current source is noncontrollable under the existing full-bridge diode rectifier structure, and it alters both the large-signal and small-signal characteristics of the dc–dc converter system. It leads to highly load-dependent steady-state dc-link and output voltages [9]. Additionally, the finite dc-link capacitance introduces a non-negligible phase delay to the small-signal response of the dc-link voltage and the phase delay further adversely affects the dynamic characteristics of the dc–dc converter [10]. Therefore, the small-signal response of the output voltage is coupled with the dc-link capacitance and shows extra phase delay [11]. A right-half-plane (RHP) zero is thereby introduced to the duty ratio-to-output voltage transfer function [12]. For example, the buck converter, which was considered a minimum-phase (no RHP zero) system, is changed into a nonminimum-phase system when it is utilized in the wireless power receiver under the series-series compensated configuration [12]. The design of the compensator becomes more challenging in the presence of RHP zeros [13]–[15]. The stability margin and dynamic response of the receiver are adversely affected [16], [17]. To improve the performance of the wireless power receivers, various control methods, e.g., the dual-side controller [1], the dual-loop controller [12], and the nonlinear controllers [18], [19] have been proposed. However, for the control method reported in [1], the performance of the receivers is still relatively poor as it is highly dependent on the length of wireless communication latency, of which neither a fast dynamic response nor large stability margin can be attained. For the control method reported in [12], the stability margin remains limited. For the nonlinear control methods reported in [18] and [19], they suffer from complicated design procedures and high computation burden. These methods do not address the non-controllable input current source nature of the dc–dc converter. Therefore, RHP zeros are present in these

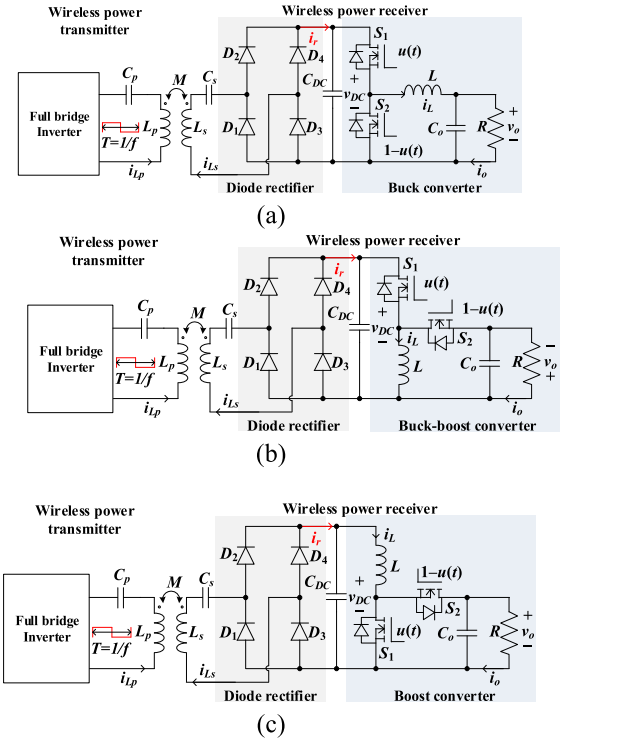

Fig. 1. Wireless power transfer systems with various receivers. (a) With full-bridge diode rectifiers and buck converter. (b) With full-bridge diode rectifiers and buck-boost converter. (c) With full-bridge diode rectifiers and boost converter.

systems and remain the limiting factor confining their stability margin and dynamic performance.

In this article, the RHP zeros of wireless power receivers using different dc–dc converters are investigated. The full-bridge rectifier adopts a different configuration, which enables certain control of the ac input current to the dc–dc converter. In doing so, RHP zeros can be subsequently eliminated, thereby improving the closed-loop bandwidth and stability margin of the wireless power receiver system.

II. RHP Zeros of the Wireless Power Receivers

A. Wireless Power Receivers

Fig. 1 shows the wireless power transfer systems with the various possible types of wireless receivers. On the transmitter side, a full-bridge inverter operating at switching frequency f ($f = 1/T$) and a primary-side transmitter coil L_p with a series compensation capacitor C_p (i.e., $1/\sqrt{C_p L_p} = 2\pi f$) are used. On the receiver side, the secondary-side receiver coil L_s with a series compensation capacitor C_s (i.e., $1/\sqrt{C_s L_s} = 2\pi f$), a passive diode rectifier (D_1 to D_4) for rectification, and a second-stage dc–dc converter for matching the voltage of the load are used. The wireless power receivers with typical dc–dc converters (i.e., the buck converter, buck-boost converter, and boost converter) are shown in Fig. 1 (a)–(c), respectively.

Due to the series-series compensation, the wireless power receiver coil L_s introduces an independent sinusoidal current $i_{Ls}(t)$ to the diode rectifier [7], [8], i.e.,

where I_{Ls} is the amplitude of the sinusoidal current $i_{Ls}(t)$. The independent current source nature and finite dc-link capacitor introduce RHP zeros to the second-stage dc–dc converters.

B. Transfer Functions and the RHP Zeros

To facilitate the analysis, the dc–dc converters share identical notations i.e., complementary MOSFET switches S_1 and S_2, inductor L, output capacitor C_o and load R. The switching functions of the switch S_1 and the complementary switch S_2 are $u(t)$ and $1-u(t)$, respectively. The switching function $u(t)$ is written as

$$u\ (t) = \begin{cases} 1 \text{ if } nT < t \le (n + D_{\text{DC-DC}})\,T \\ 0 \text{ if } (n + D_{\text{DC-DC}})\,T < t \le (n+1)\,T \end{cases} \tag{2}$$

where logic 1 and 0 represent, respectively, the ON and OFF state of the switch. Particularly, $D_{\text{DC-DC}}$ represents the duty ratio of $u(t)$ over one switching period T, and n is an arbitrary nonnegative integer. In addition, to avoid the beat frequency oscillation and ease of the analysis, the switching frequency of $u(t)$ is synchronized at f, in a cycle-by-cycle manner [20].

1) Wireless Power Receiver With Buck Converter: The state-space equation of the wireless power receiver with buck converter is written as

$$\begin{bmatrix} \frac{\partial \langle v_{\text{DC}} \rangle_T}{\partial t} \\ \frac{\partial \langle i_L \rangle_T}{\partial t} \\ \frac{\partial \langle v_o \rangle_T}{\partial t} \end{bmatrix} = \begin{bmatrix} 0 & -\frac{D_{\text{DC-DC}}}{C_{DC}} & 0 \\ \frac{D_{\text{DC-DC}}}{L} & 0 & -\frac{1}{L} \\ 0 & \frac{1}{C_o} & -\frac{1}{RC_o} \end{bmatrix} \begin{bmatrix} \langle v_{\text{DC}}(t) \rangle_T \\ \langle i_L \rangle_T \\ \langle v_o \rangle_T \end{bmatrix} + \begin{bmatrix} \frac{2I_{Ls}}{\pi C_{\text{DC}}} \\ 0 \\ 0 \end{bmatrix} \tag{3}$$

where $<v_{DC}>_T$, $<i_L>_T$, and $<v_o>_T$, respectively, represent the average of $v_{\text{DC}}(t)$, $i_L(t)$, and $v_o(t)$ over one switching cycle T. The control variable $D_{\text{DC-DC}}$ of the dc–dc converter is highlighted. Via small-signal linearization with respect to the control variable $D_{\text{DC-DC}}$ [16], the control-to-output voltage transfer function is

$$G_{\text{buck}}(s) = \frac{2RI_{Ls}\left(C_{\text{DC}}Rs - {D_{\text{DC-DC}}}^2\right)}{\left[\pi {D_{DC-DC}}^2\left[C_oC_{\text{DC}}LRs^3 + C_{\text{DC}}Ls^2 + \left(C_oR{D_{\text{DC-DC}}}^2 + C_{\text{DC}}R\right)s + {D_{\text{DC-DC}}}^2\right]\right]}. \tag{4}$$

There is one RHP zero in the transfer function, which is

$$Z_{\text{buck}} = \frac{{D_{\text{DC-DC}}}^2}{C_{\text{DC}}R} \tag{5}$$

2) Wireless Power Receiver With Buck-Boost Converter: Likewise, the state-space model of the wireless power receiver with buck-boost converter is derived as

$$\begin{bmatrix} \frac{\langle \partial v_{\text{DC}} \rangle_T}{\partial t} \\ \frac{\partial \langle i_L \rangle_T}{\partial t} \\ \frac{\partial \langle v_o \rangle_T}{\partial t} \end{bmatrix} = \begin{bmatrix} 0 & -\frac{D_{\text{DC-DC}}}{C_{\text{DC}}} & 0 \\ \frac{D_{\text{DC-DC}}}{L} & 0 & \frac{D_{\text{DC-DC}}-1}{L} \\ 0 & \frac{1-D_{\text{DC-DC}}}{C_o} & -\frac{1}{RC_o} \end{bmatrix} \times \begin{bmatrix} \langle v_{\text{DC}}(t) \rangle_T \\ \langle i_L \rangle_T \\ \langle v_o \rangle_T \end{bmatrix} + \begin{bmatrix} \frac{2I_{Ls}}{\pi C_{\text{DC}}} \\ 0 \\ 0 \end{bmatrix}. \tag{6}$$

Its control-to-output transfer function can be derived as

$$G_{\text{buck-boost}}(s) = \frac{-2RI_{Ls}\left(C_{\text{DC}}LD_{\text{DC-DC}}s^2 - C_{\text{DC}}R(1-D_{\text{DC-DC}})^2 s + D_{\text{DC-DC}}{}^2\right)}{\pi D_{\text{DC-DC}}{}^2\left[C_oC_{\text{DC}}LRs^3 + C_{\text{DC}}Ls^2 + \left(C_oD_{\text{DC-DC}}{}^2 + C_{\text{DC}}(1-D_{\text{DC-DC}})^2\right)Rs + D_{\text{DC-DC}}{}^2\right]}. \quad (7)$$

There are two RHP zeros in the transfer function, which are

$$Z_{\text{buck-boost},1} = \frac{C_{\text{DC}}R(1-D_{\text{DC-DC}})^2 + \sqrt{\left[C_{\text{DC}}R(1-D_{\text{DC-DC}})^2\right]^2 - 4(D_{\text{DC-DC}})^3C_{\text{DC}}L}}{2C_{\text{DC}}LD_{\text{DC-DC}}}$$

$$Z_{\text{buck-boost},1} = \frac{C_{DC}R(1-D_{\text{DC-DC}})^2 - \sqrt{\left[C_{\text{DC}}R(1-D_{\text{DC-DC}})^2\right]^2 - 4(D_{\text{DC-DC}})^3C_{\text{DC}}L}}{2C_{\text{DC}}LD_{\text{DC-DC}}}. \quad (8)$$

3) Wireless Power Receiver With Boost Converter: The state-space model of the wireless power receiver with boost converter is

$$\begin{bmatrix} \frac{\partial\langle v_{\text{DC}}\rangle_T}{\partial t} \\ \frac{\partial\langle i_L\rangle_T}{\partial t} \\ \frac{\partial\langle v_o\rangle_T}{\partial t} \end{bmatrix} = \begin{bmatrix} 0 & -\frac{1}{C_{\text{DC}}} & 0 \\ \frac{1}{L} & 0 & -\frac{1-\boldsymbol{D}_{\text{DC-DC}}}{L} \\ 0 & \frac{1-\boldsymbol{D}_{\text{DC-DC}}}{C_o} & -\frac{1}{RC_o} \end{bmatrix} \times \begin{bmatrix} \langle v_{\text{DC}}(t)\rangle_T \\ \langle i_L\rangle_T \\ \langle v_o\rangle_T \end{bmatrix} + \begin{bmatrix} \frac{2I_{Ls}}{\pi C_{\text{DC}}} \\ 0 \\ 0 \end{bmatrix}. \quad (9)$$

Its control-to-output transfer function can be derived as

$$G_{\text{boost}}(s) = \frac{-2RI_{Ls}\left(C_{\text{DC}}Ls^2 - C_{\text{DC}}R(1-D_{\text{DC-DC}})^2 s + 1\right)}{\pi\left[C_oC_{\text{DC}}LRs^3 + C_{\text{DC}}Ls^2 + \left(C_o + C_{\text{DC}}(1-D_{\text{DC-DC}})^2\right)Rs + 1\right]}. \quad (10)$$

Here, there are two RHP zeros, which are

$$Z_{\text{boost},1} = \frac{C_{\text{DC}}R(1-D_{\text{DC-DC}})^2 + \sqrt{\left[C_{\text{DC}}R(1-D_{\text{DC-DC}})^2\right]^2 - 4C_{\text{DC}}L}}{2C_{\text{DC}}L}$$

$$Z_{\text{boost},2} = \frac{C_{\text{DC}}R(1-D_{\text{DC-DC}})^2 - \sqrt{\left[C_{\text{DC}}R(1-D_{\text{DC-DC}})^2\right]^2 - 4C_{\text{DC}}L}}{2C_{\text{DC}}L}. \quad (11)$$

The physical origin of the RHP zeros is attributed to the non-controllable nature of diode rectifier and the current source input due to series-series compensation. As the load power changes, the dc–dc converter must adjust its duty ratio to meet the requirement of the load. However, as the input current to the receiver is noncontrollable by the converter itself (and can only be controlled at the transmitter side), the converter cannot immediately adjust the input power to meet the load power requirement. This causes a temporary power imbalance and phase delay in the output voltage response. The temporary power imbalance and phase delay in output voltage response are the origins of the RHP zeros [12]. They impose fundamental limitations to the bandwidth of the closed-loop system, and adversely affect the dynamic response and stability margin [16], [17]. To ensure sufficient phase and gain margin, the closed-loop bandwidth must be reduced, which thereby results in a slower dynamic response of the receiver. Moreover, due to the high-frequency amplification nature of RHP zeros, high-frequency disturbances may easily generate oscillation and may severely affect the system's stability.

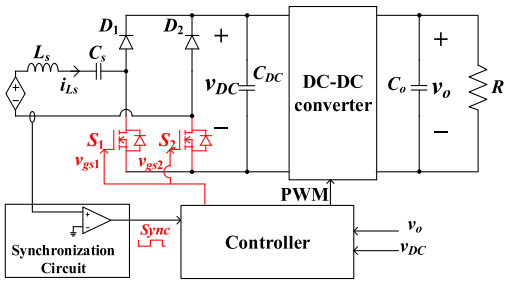

Fig. 2. Modified wireless power receiver.

III. Circuit Modifications and RHP Zeros Elimination

A. Modified Wireless Power Receiver With Active Rectifier

The proposed modified rectifier enables output regulation to be more easily attainable via the control of the input current. It is through the proper control of the input current that the RHP zeros can be eliminated. Various types of active rectifiers [21]–[23] can be adopted to enable the function of ac input current control of the receiver. Considering the popularity of the full-bridge diode rectifier, it is adopted in this article the two ground-referenced active switches type of full-bridge diode rectifier, as shown in Fig. 2, for the investigation. An external synchronization circuit is used to convert the ac current i_{Ls} into a square wave for the controller [20]. To reduce switching loss, the rising edge of the gate driving signals are aligned with the zero crossing points of i_{Ls}, and thereby the switches S_1 and S_2 can operate with zero voltage switching (ZVS) with reduced switching loss. In addition, the introduced switches cause less conduction loss as compared with diodes. The modification will not deteriorate the efficiency of the receiver system. Moreover, the cascaded dc–dc converter can operate with fixed duty ratio to match the voltage difference between the dc-link voltage and output voltage, which may further increase the efficiency of the dc–dc converter. Both the duty ratios of the gate driving signal v_{gs1} and v_{gs2} are D ($0.5 \leq D \leq 1$), and they are 180° phase shift with one another. Figs. 3 and 4, respectively, show the equivalent circuit models and key forms in different operation states.

1) *State I* [$nT \leq t < (n+D-0.5)T$]: Fig. 3(a) shows the equivalent circuit model of the power circuit in state I. At $t = nT$, S_2 turns ON with ZVS. During state I, both switches are ON. The ac current i_{Ls} is freewheeled and no current flows to the dc-link capacitor.
2) *State II* [$(n+D-0.5)T \leq t < (n+0.5)T$]: Fig. 3(b) shows the equivalent circuit model of the power circuit in state II. At $t = (n+D-0.5)T$, S_1 turns OFF and D_1 turns ON. During state II, $i_{Ls}(t)$ flows to the dc-link capacitor.
3) *State III* [$(n+0.5)T \leq t < (n+D)T$]: Fig. 3(c) shows the equivalent circuit model of the power circuit in state III. At $t = (n+0.5)T$, S_1 turns ON with ZVS. During state III,

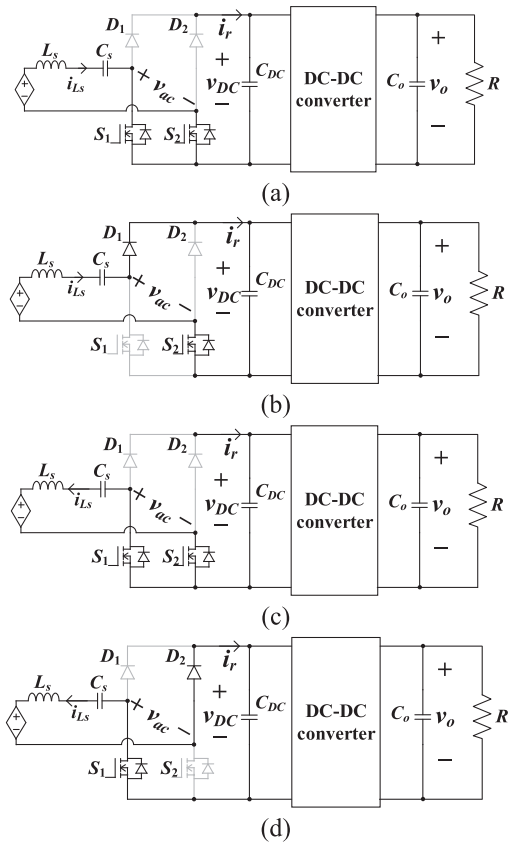

Fig. 3. Equivalent circuit models of the modified wireless power receiver in different operation states. (a) Equivalent circuit model of State I. (b) Equivalent circuit model of State II. (c) Equivalent circuit model of State III. (d) Equivalent circuit model of State IV.

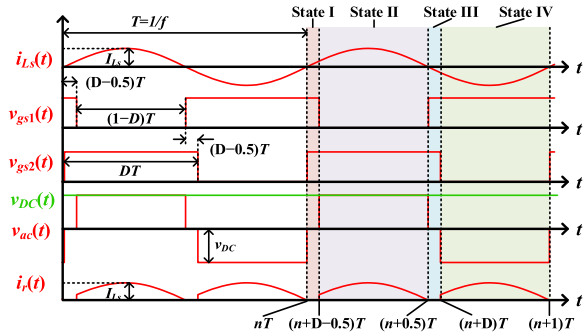

Fig. 4. Key waveforms of the wireless power receiver system.

both switches are ON. i_{Ls} is freewheeled and no current flows to the dc-link capacitor.

4) *State IV* $[(n+D)T \le t < (n+1)T]$: Fig. 3(d) shows the equivalent circuit model of the power circuit in state III. At $t = (n+D)T$, S_2 turns OFF and e D_1 turns ON. During state IV, $i_{Ls}(t)$ flows to the dc-link capacitor.

In general, the average current i_{rT} flows to the dc-link capacitor can be obtained as

$$\langle i_r \rangle_T = \frac{1}{T}\int_{nT}^{(n+1)T} i_r(t)\,dt = \frac{I_{Ls}}{\pi}\left(1-\cos(2\pi D)\right). \quad (12)$$

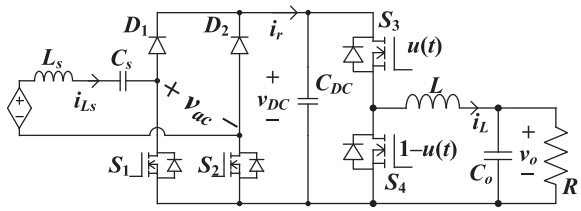

Fig. 5. Modified wireless power receiver with buck converter.

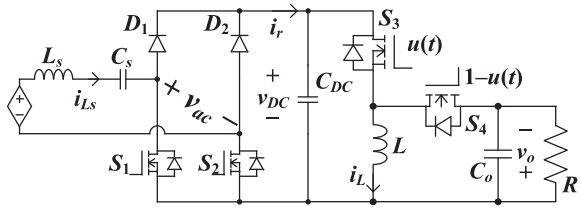

Fig. 6. Modified wireless power receiver with buck-boost converter.

B. Averaged Model and Small-Signal Model

1) Modified Wireless Power Receiver With Buck Converter: Fig. 5 shows the schematic diagram of the modified wireless power receiver with buck converter. The state-space averaged model is derived as

$$\begin{bmatrix} \frac{\partial\langle v_{\rm DC}\rangle_T}{\partial t} \\ \frac{\partial\langle i_L\rangle_T}{\partial t} \\ \frac{\partial\langle v_o\rangle_T}{\partial t} \end{bmatrix} = \begin{bmatrix} 0 & -\frac{D_{\rm DC-DC}}{C_{\rm DC}} & 0 \\ \frac{D_{\rm DC-DC}}{L} & 0 & -\frac{1}{L} \\ 0 & \frac{1}{C_o} & -\frac{1}{RC_o} \end{bmatrix} \times \begin{bmatrix} \langle v_{\rm DC}(t)\rangle_T \\ \langle i_L\rangle_T \\ \langle v_o\rangle_T \end{bmatrix} + \begin{bmatrix} \frac{[1-\cos(2\pi \boldsymbol{D})]I_{Ls}}{\pi C_{\rm DC}} \\ 0 \\ 0 \end{bmatrix}. \quad (13)$$

The control variable of the active rectifier D is in bold. The control-to-output voltage transfer function of the modified wireless power receiver with buck converter is

$$G_{M_{\rm buck}}(s) = \frac{2D_{\rm DC-DC}I_{Ls}R\sin(2\pi D)}{\left[C_oC_{\rm DC}LRs^3+C_{\rm DC}Ls^2+\left(C_oRD_{\rm DC-DC}{}^2+C_{\rm DC}R\right)s+D_{\rm DC-DC}{}^2\right]}. \quad (14)$$

2) Modified Wireless Power Receiver With Buck-Boost Converter: Fig. 6 shows the schematic diagram of the modified wireless power receiver with the buck-boost converter. The state-space averaged model is

$$\begin{bmatrix} \frac{\partial\langle v_{\rm DC}\rangle_T}{\partial t} \\ \frac{\partial\langle i_L\rangle_T}{\partial t} \\ \frac{\partial\langle v_o\rangle_T}{\partial t} \end{bmatrix} = \begin{bmatrix} 0 & -\frac{D_{\rm DC-DC}}{C_{\rm DC}} & 0 \\ \frac{D_{\rm DC-DC}}{L} & 0 & -\frac{1-D_{\rm DC-DC}}{L} \\ 0 & \frac{1-D_{\rm DC-DC}}{C_o} & -\frac{1}{RC_o} \end{bmatrix} \times \begin{bmatrix} \langle v_{\rm DC}(t)\rangle_T \\ \langle i_L\rangle_T \\ \langle v_o\rangle_T \end{bmatrix} + \begin{bmatrix} \frac{[1-\cos(2\pi \boldsymbol{D})]I_{Ls}}{\pi C_{\rm DC}} \\ 0 \\ 0 \end{bmatrix}. \quad (15)$$

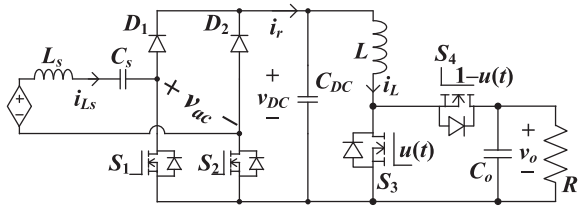

Fig. 7. Modified wireless power receiver with boost converter.

Its control-to-output transfer function is derived as

$$G_{M_{\text{buck-boost}}}(s) = \frac{2D_{\text{DC-DC}}I_{Ls}R\sin(2\pi D)(1-D_{\text{DC-DC}})}{\left[\begin{array}{c}\left[C_oC_{\text{DC}}LRs^3+C_{\text{DC}}Ls^2+\right.\\ \left.\left(C_o{D_{\text{DC-DC}}}^2+C_{\text{DC}}(1-D_{\text{DC-DC}})^2\right)Rs+{D_{\text{DC-DC}}}^2\right]\end{array}\right]}. \quad (16)$$

3) Modified Wireless Power Receiver With Boost Converter: Fig. 7 shows the schematic diagram of the modified wireless power receiver with boost converter. The state-space averaged is

$$\begin{bmatrix}\frac{\partial\langle v_{\text{DC}}\rangle_T}{\partial t}\\ \frac{\partial\langle i_L\rangle_T}{\partial t}\\ \frac{\partial\langle v_o\rangle_T}{\partial t}\end{bmatrix} = \begin{bmatrix}0 & -\frac{1}{C_{\text{DC}}} & 0\\ \frac{1}{L} & 0 & -\frac{1-D_{\text{DC-DC}}}{L}\\ 0 & \frac{1-D_{\text{DC-DC}}}{C_o} & -\frac{1}{RC_o}\end{bmatrix}\begin{bmatrix}\langle v_{\text{DC}}(t)\rangle_T\\ \langle i_L\rangle_T\\ \langle v_o\rangle_T\end{bmatrix} + \begin{bmatrix}\frac{[1-\cos(2\pi D)]I_{Ls}}{\pi C_{\text{DC}}}\\ 0\\ 0\end{bmatrix}. \quad (17)$$

Its control-to-output transfer function is

$$G_{M\text{boost}}(s) = \frac{2I_{Ls}R\sin(2\pi D)(1-D_{\text{DC-DC}})}{\left[C_oC_{\text{DC}}LRs^3+C_{\text{DC}}Ls^2+\left(C_o+C_{\text{DC}}(1-D_{\text{DC-DC}})^2\right)Rs+1\right]}. \quad (18)$$

As compared with the state-space equations of the original wireless power receivers (3), (6), (9) and modified wireless power receivers (13), (15), and (17), the major difference is that the control variable $D_{\text{DC-DC}}$ of the original ones is embedded in the state matrix and coupled with the state variables, while the control variable D of the modified ones is located at the input matrix and decoupled with the state variables. Via decoupling the control variables from the state variables, the RHP zeros can be removed.

To verify the accuracy of the models, the circuit simulation results carried out using PSIM v2020a, and the theoretical results (4), (7), (10), (14), (16), and (18) are plotted altogether as shown in Fig. 8. The parameters used are $I_{Ls} = 1$ A, $C_{\text{DC}} = 30$ μF, $L = 77$ μH, $C_o = 40$ μF, $R = 7$, $D_{\text{DC-DC}} = 0.5$, and $D = 0.51$. Fig. 8 (a)–(c), respectively, shows the theoretical and simulated Bode plots of the transfer functions of the original and modified wireless power receivers with buck converter, buck-boost converter, and boost converter. The simulated and the theoretical results are in close agreement, validating the accuracy of the models.

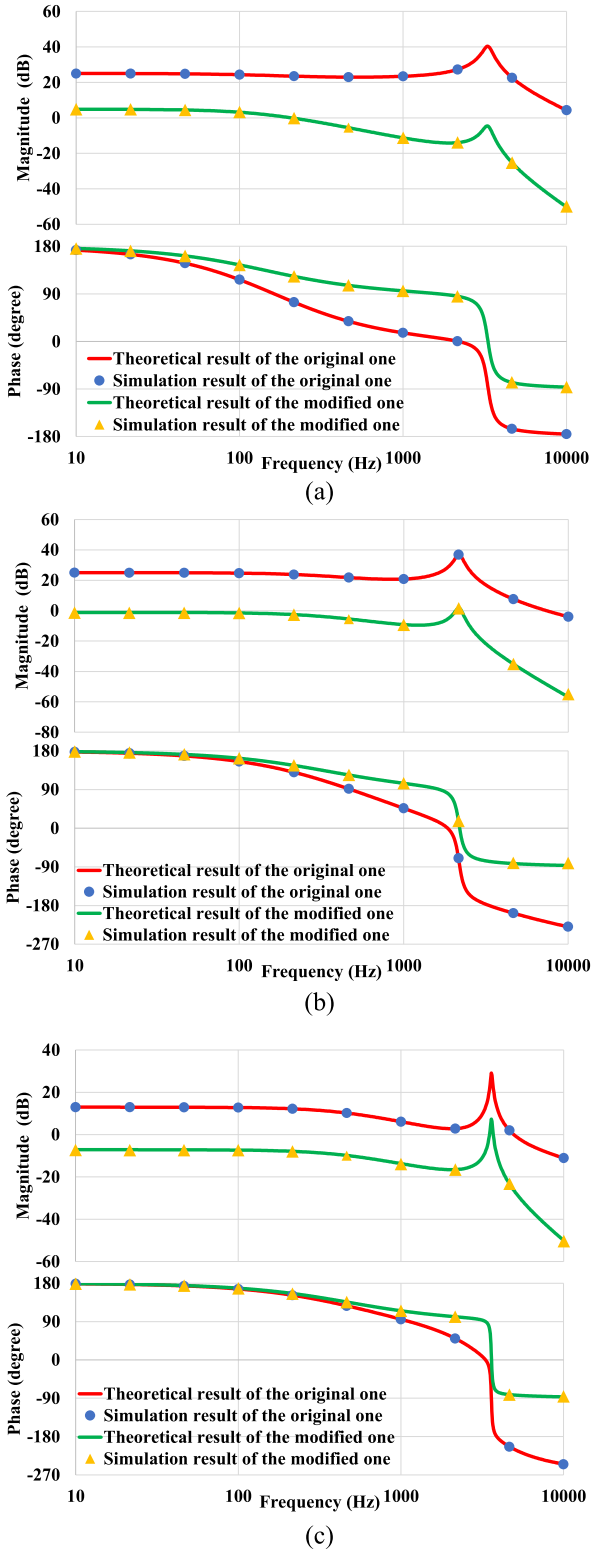

Fig. 8. Theoretical and simulated Bode plots the transfer functions of the wireless power receivers. (a) Wireless power receivers with buck converter. (b) Wireless power receivers with buck-boost converter. (c) Wireless power receivers with buck-boost converter.

Moreover, Fig. 9 (a)–(c) shows the pole-zero maps of the transfer functions of the original and modified wireless power receivers. The pole-zero maps of the wireless power receivers show that the RHP zeros are eliminated by using modified wireless power receivers. In addition, as compared with the

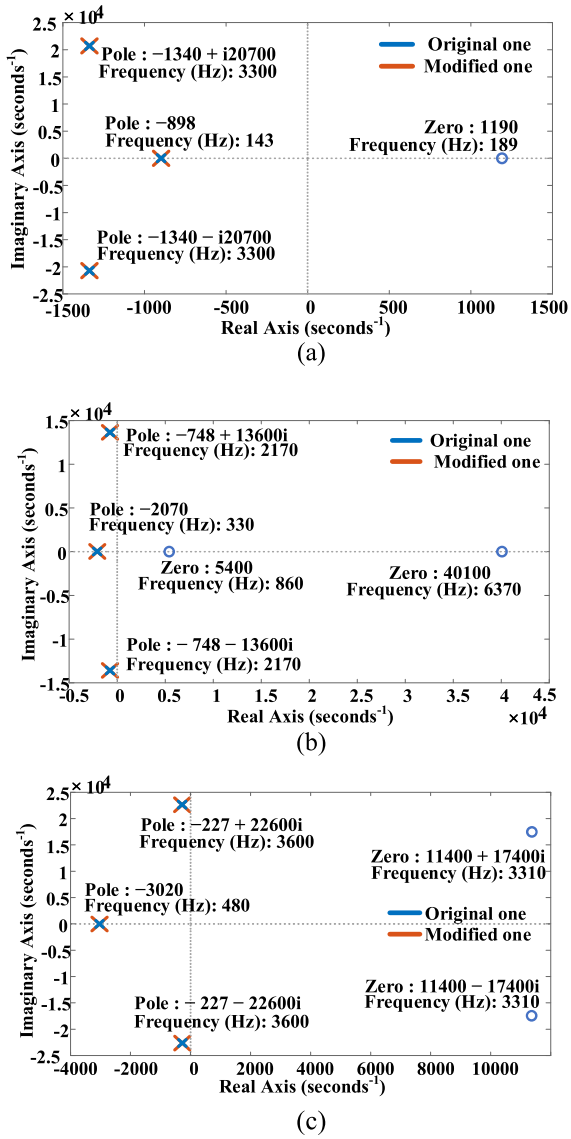

Fig. 9. Pole-zero maps of the transfer functions of the wireless power receivers. (a) Wireless power receivers with buck converter. (b) Wireless power receivers with buck-boost converter. (c) Wireless power receivers with boost converter.

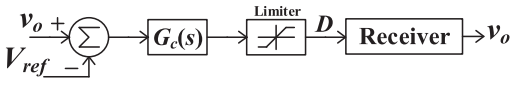

Fig. 10. Block diagram of the closed-loop system.

original ones [see (4), (7), and (10)], the transfer functions of the modified wireless power receiver [see(14), (16), and (18)] show that the RHP zero are eliminated without affecting the poles.

IV. Dynamic Performance Improvement

The stability and dynamic response of wireless power receivers with single-loop feedback control (see Fig. 10) is assessed, of which a proportional-integral (PI) compensator $G_c(s)$ is used to achieve output voltage regulation. The transfer function of the PI compensator is

$$G_c\ (s) = k_p\ + \frac{k_i}{s} \tag{19}$$

where k_p and k_i are the proportional gain and integral gain, respectively.

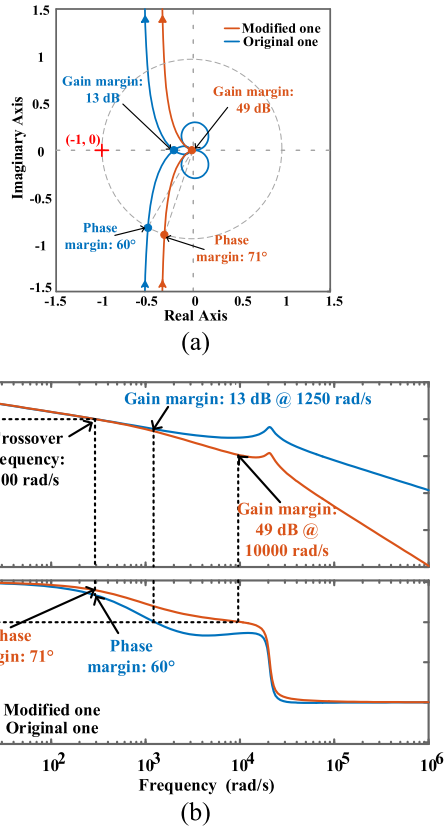

Fig. 11. Bode plots of loop gains of the modified and original wireless power receivers with buck converter. (a) Nyquist plots of the loop gains. (b) Bode plots of the loop gains.

A. Closed-Loop Stability Assessment

To have a fair assessment of the closed-loop stability, the compensators are designed such that the crossing frequency of loop gains of wireless power receivers are located at the same frequency. To ensure sufficient stability margin for both the original and modified wireless power receivers, the crossing frequency is chosen at around 1/4 of the RHP zero [1190 rad/s, see Fig. 9(a)] of the buck converter. Consequently, the crossing frequency is selected at 300 rad/s.

Fig. 11 shows the characteristics of the loop gains of the original and modified wireless power receivers with buck converter. The parameters of the compensator of the original receiver are $D_{DC\text{-}DC}$=0.5, $k_p = 0.0027284$, and $k_i = 17.1836$, and that of the modified receiver are $D_{DC\text{-}DC}$=0.5, D=0.51, $k_p = 0$, and $k_i = 179.8716$. Fig. 11(a) shows no encirclement of $(-1, 0)$, suggesting that both receivers are stable. Fig. 11(b) shows that the modified one features a phase margin of 71° at 300 rad/s, and a gain margin of 49 dB at 10000 rad/s, while the original

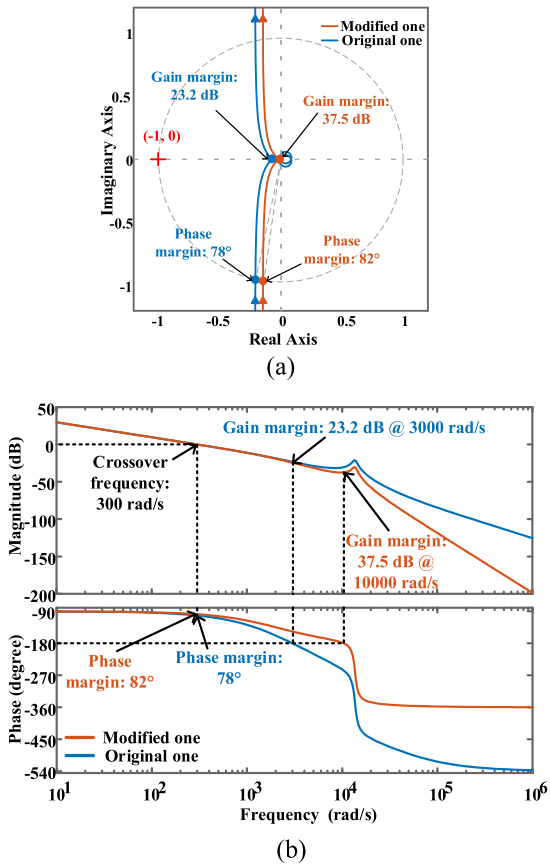

Fig. 12. Bode plots of loop gains of the modified and original wireless power receivers with buck-boost converter. (a) Nyquist plots of the loop gains. (b) Bode plots of the loop gains.

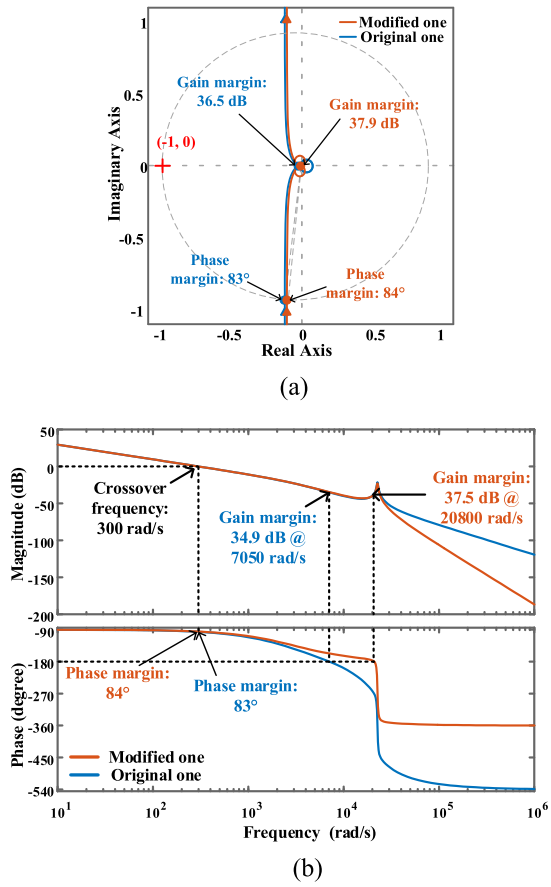

Fig. 13. Bode plots of loop gains of the wireless power receivers. (a) Nyquist plots of the loop gains. (b) Bode plots of the loop gains.

wireless power receiver features a phase margin of 60° at 300 rad/s and a gain margin of 13 dB at 1250 rad/s.

Fig. 12 shows the characteristics of the loop gains of the original and modified wireless power receivers with buck-boost converter. The parameters of the compensator are $D_{DC\text{-}DC}$= 0.5, k_p= 0, k_i= 16.97 (original receiver) and $D_{DC\text{-}DC}$= 0.5, D= 0.51, k_p= 0, k_i= 344.6537 (modified receiver). Fig. 12(a) shows no encirclement of $(-1, 0)$, suggesting that both receivers are stable. Fig. 12(b) shows that the modified one features a phase margin of 82° at 300 rad/s, and a gain margin of 37.5 dB at 10000 rad/s, while the original wireless power receiver features a phase margin of 78° at 300 rad/s and a gain margin of 23.2 dB at 3000 rad/s.

Fig. 13 shows the characteristics of the loop gains of the original and modified wireless power receivers with boost converter. The parameters of the compensator are $D_{DC\text{-}DC}$= 0.5, k_p = 0, k_i = 67.64 (original receiver) and $D_{DC\text{-}DC}$= 0.5, D= 0.51, k_p = 0, k_i = 685.7861 (modified receiver). Fig. 13(a) shows no encirclement of $(-1, 0)$, suggesting that both receivers are stable. Fig. 13(b) shows that the modified one features a phase margin of 84° at 300 rad/s, and a gain margin of 37.5 dB at 20800 rad/s, while the original wireless power receiver features a phase margin of 83° at 300 rad/s and a gain margin of 34.9 dB at 7050 rad/s.

In general, both the original and modified wireless power receivers are stable. However, the modified ones show larger phase margins and gain margins, suggesting improved stability margins.

B. Dynamic Response Assessment

For fair assessment of dynamic responses, the compensator is designed such that the set of phase margin and gain margin of wireless power receivers are identical.

Fig. 14(a) shows the Bode plots of the loop gains of the wireless power receivers with buck converter, where both receivers share identical gain margin of 20 dB and phase margins of 76.8°. The parameters of the compensator are $D_{DC\text{-}DC}$= 0.5, k_p= 0, k_i= 6.64 (original receiver) and $D_{DC\text{-}DC}$= 0.5, D= 0.523, k_p= 0.0732, k_i= 130.25 (modified receiver). However, the modified one achieves a higher crossover frequency of 480 rad/s, while the original one achieves a relatively low crossover frequency of 118 rad/s. Fig. 14(b) shows the time-domain response of voltage reference step change from 8 to 8.8 V. The modified one reaches the new reference value faster than the original one. These results validate that the modified wireless power receiver can improve the dynamic response.

Fig. 15(a) shows the Bode plots of the loop gains of the wireless power receivers with buck-boost converter, where both receivers are compensated such that they have identical gain

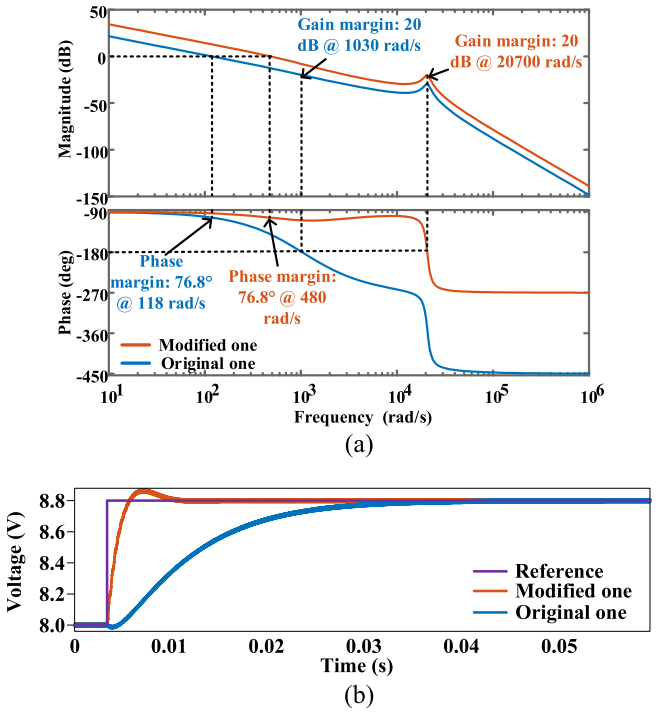

Fig. 14. Frequency-domain and time-domain responses of the original and modified wireless power receivers with buck converter. (a) Bode plots of the loop gains. (b) Time-domain waveforms of reference tracking.

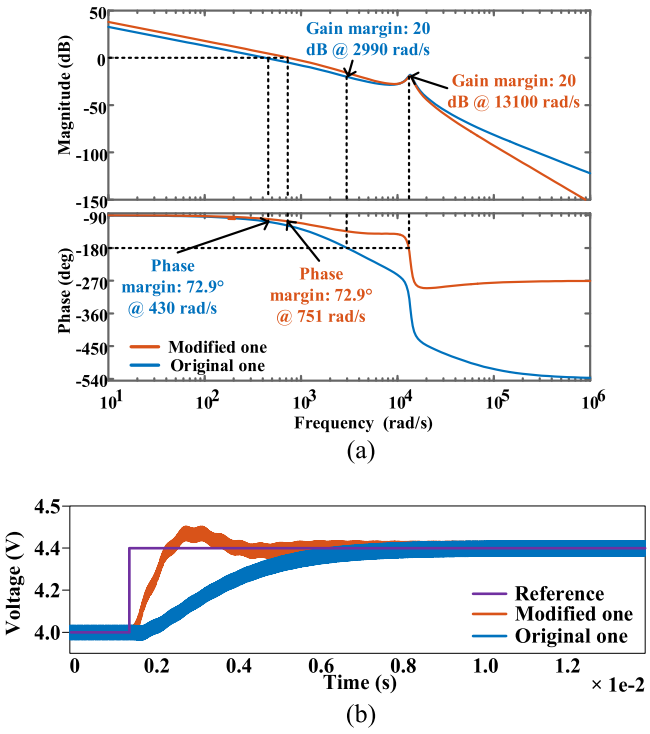

Fig. 15. Frequency-domain and time-domain responses of the original and modified wireless power receivers with buck-boost converter. (a) Bode plots of the loop gains. (b) Time-domain waveforms of reference tracking.

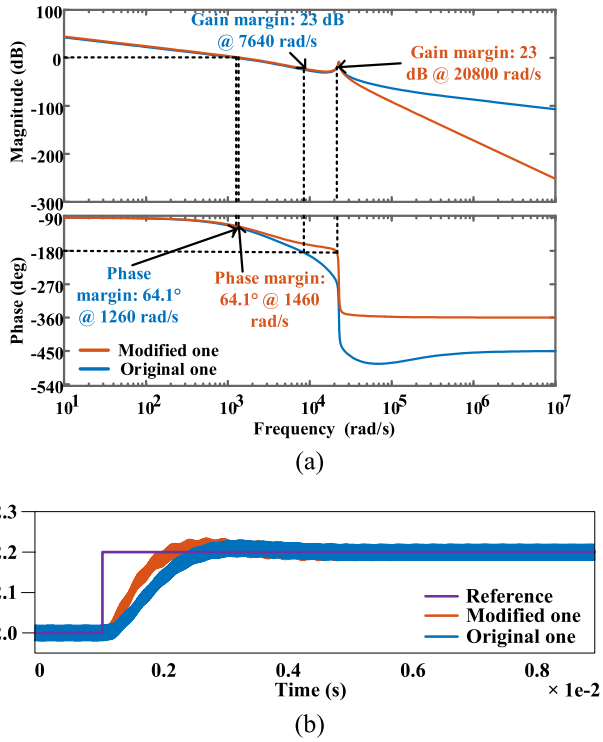

Fig. 16. Frequency-domain and time-domain responses of the original and modified wireless power receivers with boost converter. (a) Bode plots of the loop gains. (b) Time-domain waveforms of reference tracking.

margins of 20 dB and phase margins of 72.9°. The parameters of the compensator are $D_{DC\text{-}DC}$= 0.5, $k_p = 0$, $k_i = 24.53$ (original receiver) and $D_{DC\text{-}DC}$= 0.5, D= 0.54, k_p = 0.0167 and k_i = 228.36 (modified receiver). However, the modified one achieves a higher crossover frequency of 751 rad/s, while the original one achieves a relatively low crossover frequency of 430 rad/s. Fig. 15(b) response of voltage reference step change from 4 V to 4.4 V. The modified one reaches the new reference value faster than the original one. These results validate that the modified wireless power receiver can improve the dynamic response.

Fig. 16(a) shows the Bode plots of the loop gains of the wireless power receivers with boost converter, where both receivers are compensated such that they have identical gain margins of 23 dB and phase margins of 64.1°. The parameters of the compensator are $D_{DC\text{-}DC}$= 0.5, k_p = 0.002777, k_i = 305.8 (original receiver) and $D_{DC\text{-}DC}$= 0.5, D= 0.55, $k_p = 0$, $k_i = 745.744$ (modified receiver). However, the modified one achieves a higher crossover frequency of 1460 rad/s, while the original one achieves a relatively low crossover frequency of 1260 rad/s. Fig. 16(b) shows the time-domain response of voltage reference step change from 2 to 2.2 V. The modified one reaches the new reference value slightly faster than the original one. These results show that the modified wireless power receiver can improve the dynamic response.

V. Experimental Verification

Fig. 17 shows the experimental setup, of which an MSXO3024A oscilloscope, N2873 passive voltage probes, N2790A differential voltage probes, and 1147B current probes

TABLE I
LIST OF COMPONENTS

Component / Parameters	Value / Part Number
L_s	103 μH Hand-made
C_s	24 nF B32672L1123J000×2
C_{DC}	30 μF CL32B106KBJNNNE×3
L	77 μH Hand-made
C_o	40 μF CL32B106KBJNNNE×4
Gate Driver	ADuM3223
MOSFET (S_1, S_2)	IPP055N03LGXKSA1
MOSFET (S_3, S_4)	IRLU3714ZPBF
Diode (D_1-D_4)	IPP055N03LGXKSA1
MCU	LAUNCHXL-F28379D

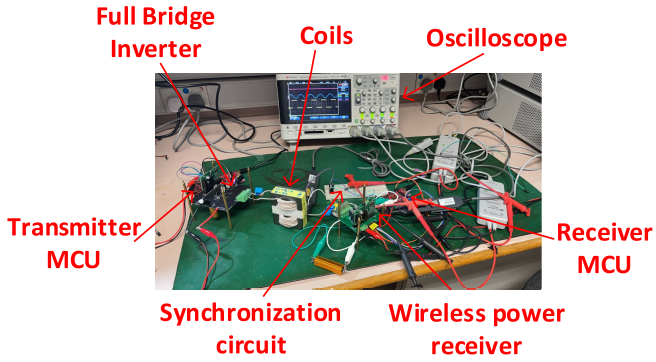

Fig. 17. Photograph of the prototype and the experimental setup.

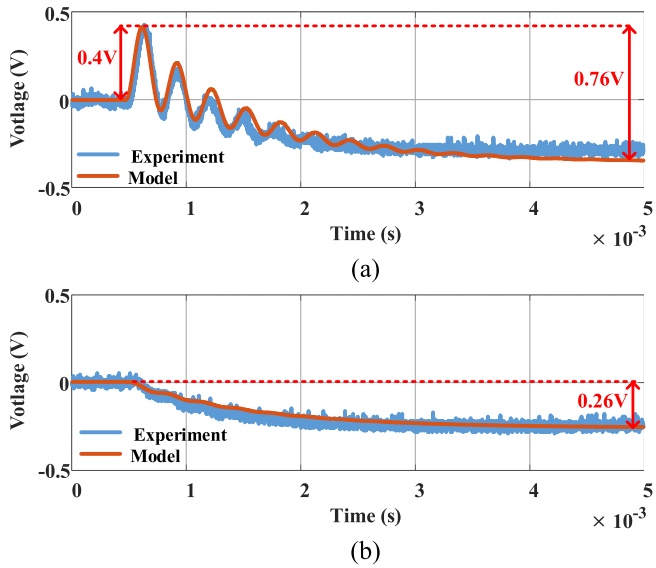

Fig. 18. Output voltage waveforms of step responses of wireless power receivers. (a) Wireless power receiver with buck converter. (b) Modified wireless power receiver with buck converter.

are used for the measurement. The modified and original wireless power receivers with buck converter are implemented and verified in the experiment. The components and parameters of the prototype are shown in Table I.

A. Open-Loop Verification

The open-loop verifications are performed under these conditions: $I_L = 1$ A, $R = 7\ \Omega$, $D_{\text{DC-DC}} = 0.5$, and $D = 0.53$. Fig. 18(a) shows the output voltage waveform v_o of the wireless power receivers with buck converter in response to the step change of $D_{\text{DC-DC}}$ from 0.5 to 0.52. The output voltage of the wireless power receiver with buck converter shows an inverse response [see Fig. 18(a)], which initially raises by 0.4 V, then drops by 0.76 V, and eventually reaches the new steady-state value. This inverse response behavior signifies the presence of the RHP zero [12], [16]. Fig. 18(b) shows the output voltage waveforms v_o of the modified wireless power receiver with buck converter in response to the step change of D from 0.53 to 0.58. The output voltage does not present an inverse response [see Fig. 18(b)], which drops by 0.26 V, and eventually reaches the new steady-state value. This monotonical response qualitatively verifies the elimination of the RHP zero. Moreover, as shown in Fig. 18(a) and (b), the experimental results (in blue) are very close to the theoretical results (in red), which are simulated using the small-signal models given in (4) and (14). These results not only validate the accuracy of the models, but further verify the elimination of the RHP zero.

The experimental and theoretical Bode plots of the original and modified wireless power receiver system with buck converter are shown in Fig. 19(a) and (b), respectively. Fixed-frequency sinusoidal small-signal perturbations are injected into the control variables and the corresponding small-signal responses are measured via oscilloscope. Through repeating the measurement at different frequencies, the experimental Bode plots are obtained [12]. The experimental and theoretical results show close agreement, verifying the accuracy of the models. Moreover, comparing the Bode phase plots of Fig. 19(a) and (b), the phase drop of the modified one (from 180° to −90°) is less than that of the original one (from 180° to −180°). The reduction of 90° verifies the elimination of RHP zero.

B. Closed-Loop Verification

For fair comparison, both receivers are compensated such that the set of gain and phase margin of both systems are 20 dB and 76.8° (see Fig. 11). The implemented parameters of the compensator are $k_p = 0$ and $k_i = 6.6$ (original receiver) and $k_p = 0.07$ and $k_i = 130$ (modified receiver). Fig. 20 shows the dynamic responses of the step change of the reference voltage from 8 to 8.8 V. Both receivers can ramp up and reach the new steady-state output voltage. The original receiver features a settling time of around 25 ms without overshoot, while the modified one features a settling time of around 5 ms with a slight overshoot of 0.2 V. In general, the modified one shows five-time faster dynamic response in terms of reference tracking.

Fig. 21 shows the dynamic responses of load step changes from 8.6 to 7 Ω. Both receivers can retain regulated output voltage at 8.8 V. However, the modified one features a settling time of around 4 ms with an undershoot of 0.4 V, while, in

TABLE II
COMPARISON WITH DIFFERENT CONTROL METHODS FOR WIRELESS POWER RECEIVER

	This work	[1]	[12]	[18]	[19]
Transmitter topology	**Full-bridge inverter**	Full-bridge inverter	Full-bridge inverter	Full-bridge inverter	Full-bridge inverter
Receiver topology	**Active rectifier + DC-DC converter**	Diode rectifier + Buck converter	Diode rectifier + Buck converter	Diode rectifier + Buck converter	Diode rectifier + Buck-boost converter
Topology for regulation	**Active rectifier**	Full bridge inverter and DC-DC converter	Buck converter	Buck converter	Buck-boost converter
Regulation objective	**Output voltage**	Output voltage	Output voltage	DC-link voltage	Output voltage
Control Method	**Receiver-side single-loop control**	Dual-side control	Receiver-side dual-loop control	Receiver-side model predictive control	Receiver-side sliding mode control
Number of sensors for control scheme	**1 voltage sensor**	2 voltage sensors	2 voltage sensors	2 voltage sensors and 1 current sensor	1 voltage sensors and 1 current sensor
Theoretical basis	**RHP zero elimination**	Transmitter-side coarse adjustment & Receiver-side fine regulation	Poles cancelation	Lyapunov stability criteria	Lyapunov stability criteria
Controller parameter design	**Model-based design**	N/A	Model-based design	Empirical	Routh-Hurwitz criteria
Wireless communication	**No**	Yes	No	No	No
RHP zero	**No**	Yes	Yes	N/A	N/A
Dynamic response	**Fast**	Slow	Medium	N/A	Medium
Stability Margin	**Wide**	N/A	Medium	Wide	Wide
Features	**High performance Minimum-phase system**	Distributed control burden	Ease of implementation	Large-signal stability	Large-signal stability
Disadvantage	**Extra component cost**	Significant delay due to wireless communication	Narrow operating range	High design complexity and computation burden	High design complexity and computation burden

contrast, the original one features a settling time of around 25 ms with an undershoot of 1.6 V. The comparative study shows that the modified one features 5-time faster dynamic response and four-time smaller undershoot voltage against load disturbance.

To assess the stability margin, Fig. 22 gives the dynamic responses in response to the step change of crossover frequency, after which the crossover frequency of both receiver systems are increased to 1030 rad/s. Correspondingly, the parameters of the compensator of the original receiver are changed from $k_p = 0$ and $k_i = 6.6$ to $k_p = 0$ and $k_i = 66$, while the parameters of the compensator of the modified receiver are changed from $k_p = 0.07$ and $k_i = 130$ to $k_p = 0.175$ and $k_i = 325$. The output voltage of the original wireless power receiver with buck converter oscillates and becomes unstable, while the output voltage of the modified one remains constant and stable. This test verifies that the modified solution features a larger stability margin.

VI. COMPARISON AND DISCUSSION

A comparative study of different control methods of the wireless power receiver system is given in Table II. A dual-side control architecture for output voltage regulation where the transmitter provides the coarse adjustment, and the receiver attains fine output regulation. However, due to the latency of wireless communication (from a few milliseconds to hundreds of milliseconds [24]), the dynamic response is slow and stability margin is narrow are presented in [1]. Li *et al.* [12] present a dual-loop control method for output voltage regulation. Owing to the poles cancellation and system order reduction property, the dynamic response can be slightly improved but remains limited by the RHP zero. Zhou *et al*. [18] and Yang *et al.* [19] present nonlinear controllers for dc-link voltage and output voltage regulation, respectively. Large-signal stability can be expected, but they suffer from high design complexity and computation burden. Comparing with these methods, this article presents a general solution for output voltage regulation. Via elimination of the RHP zeros, the closed-loop bandwidth, phase margin and gain margin can be significantly improved, thereby enabling a fast dynamic response and wide stability margin.

VII. CONCLUSION

In this article, the RHP zeros of wireless power receivers with dc–dc converter are investigated. By modifying the power receiver through the use of an active diode rectifier that can control the ac input current, the inherent RHP zeros of the wireless power receivers can be eliminated to achieve good stability and dynamic response of the wireless power receivers. Our experimental studies show that the modified solution can achieve faster dynamic responses in terms of reference tracking and load disturbances under output voltage regulation. In addition, the modified receiver features a larger stability margin under the same closed-loop bandwidth. To conclude, this article presents assessments of the nonminimum characteristic of the wireless power receivers and the proposed solution enables wireless power receivers to achieve better regulation.

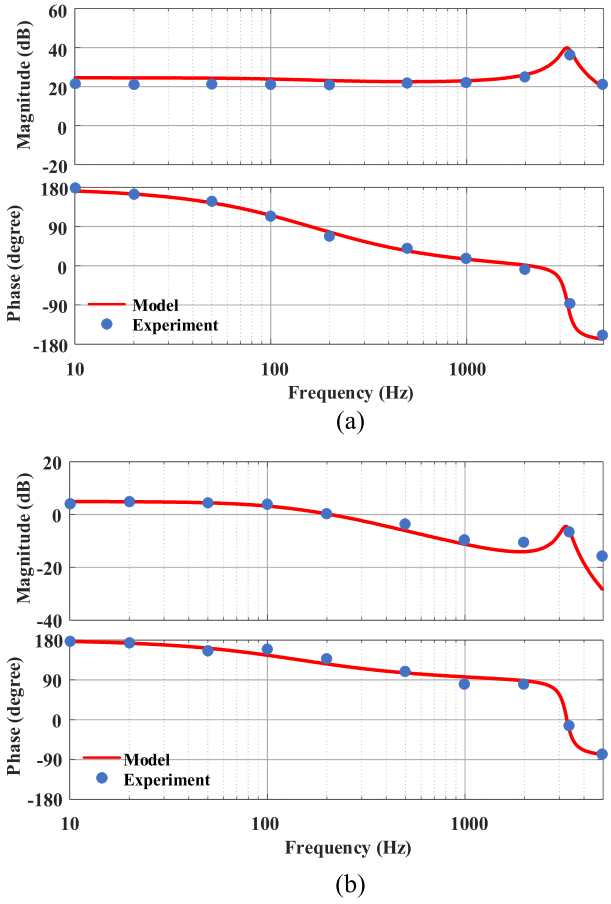

Fig. 19. Theoretical and experimental Bode plots of wireless power receivers.

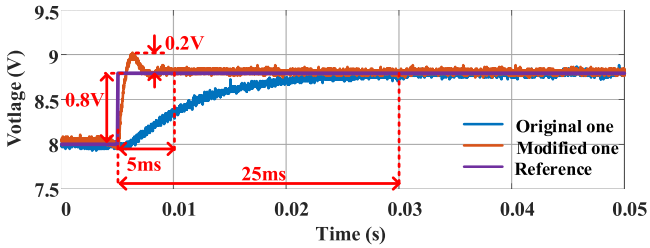

Fig. 20. Dynamic responses of the step change of the reference voltage.

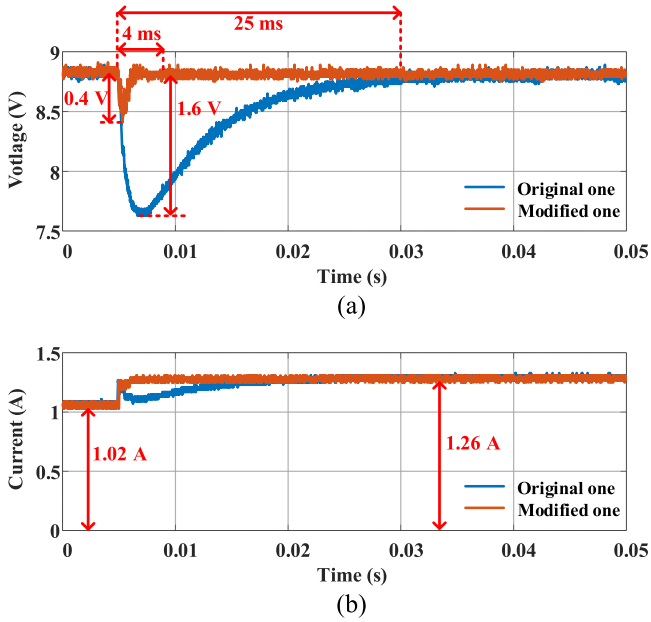

Fig. 21. Dynamic responses of load disturbances under output voltage regulation. (a) Output voltage. (b) Output current.

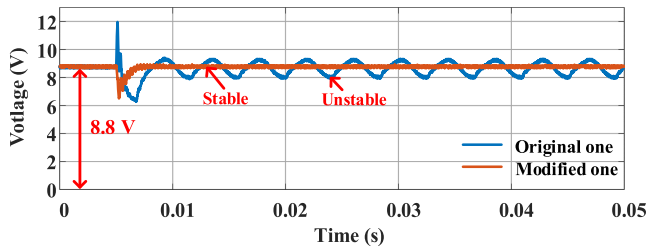

Fig. 22. Dynamic responses in response to the step change of crossover frequency.

REFERENCES

[1] "The qi wireless power transfer system power class 0 specification part 4: Reference designs," Wireless Power Consortium, Piscataway, NJ, USA, Feb. 2017.

[2] Datasheet TS51223, "TS51223 wireless power receiver", semtech, 2016. [Online]. Available: https://www.semtech.com/products/wireless-charging/linkcharge-ics/ts51223

[3] M. Fu, C. Ma, and X. Zhu, "A cascaded boost–buck converter for high-efficiency wireless power transfer systems," *IEEE Trans. Ind. Informat.*, vol. 10, no. 3, pp. 1972–1980, Aug. 2014,.

[4] A. Arora, S. Lele, N. Medora, and S. Souri, *Lithium-Ion Battery Failures in Consumer Electronics*, Norwood, MA, USA: Artech House , 2019.

[5] J. T. Boys, G. A. Covic, and Y. Xu, "DC analysis technique for inductive power transfer pick-ups," *IEEE Power Electron. Lett.*, vol. 1, no. 2, pp. 51–53, Jun. 2003,.

[6] X. Li, C.-Y. Tsui, and W.-H. Ki, "A 13.56 MHz wireless power transfer system with reconfigurable resonant regulating rectifier and wireless power control for implantable medical devices," *IEEE J. Solid-State Circuits*, vol. 50, no. 4, pp. 978–989, Apr. 2015.

[7] J. Huh, S. W. Lee, W. Y. Lee, G. H. Cho, and C. T. Rim, "Narrow-width inductive power transfer system for online electrical vehicles," *IEEE Trans. Power Electron.*, vol. 26, no. 12, pp. 3666–3679, Dec. 2011.

[8] W. Zhang, and C. C. Mi, "Compensation topologies of high-power wireless power transfer systems," *IEEE Trans. Veh. Tech.*, vol. 65, no. 6, pp. 4768–4778, Jun. 2016.

[9] Z. Li, C. Zhu, J. Jiang, K. Song, and G. Wei, "A 3-kw wireless power transfer system for sightseeing car supercapacitor charge," *IEEE Trans. Power Electron.*, vol. 32, no. 5, pp. 3301–3316, May 2017.

[10] X. Yue, X. Wang, and F. Blaabjerg, "Review of small-signal modelling methods including frequency-coupling dynamics of power converters," *IEEE Trans. Power Electron.*, vol. 34, no. 4, pp. 3313–3328, Apr. 2019.

[11] R. D. Middlebrook, "Null double injection and the extra element theorem," *IEEE Trans. Educ.*, vol. 32, no. 3, pp. 167–180, Aug. 1989.

[12] K. Li, S. C. Tan, and R. S. Y. Hui, "On effect of right-half-plane zero present in buck converters with input current source in wireless power receiver systems," *IEEE Trans. Power Electron.*, vol. 36, no. 6, pp. 6364–6374, Jun. 2021.

[13] J. B. Hoagg, and D. S. Bernstein, "Nonminimum-phase zeros - much to do about nothing - classical control - revisited part II," *IEEE Control Syst. Mag.*, vol. 27, no. 3, pp. 45–57, Jun. 2007.

[14] J. Freudenberg, and D. Looze, "Right half plane poles and zeros and design tradeoffs in feedback systems," *IEEE Trans. Automat. Control,* vol. 30, no. 6, pp. 555–565, Jun. 1985.

[15] L. Harnefors, and H. P. Nee, "Model-based current control of AC machines using the internal model control method," *IEEE Trans. Ind. Appl.*, vol. 34, no. 1, pp. 133–141, Jan./Feb. 1998.

[16] R. W. Erickson, and D. Maksimovic, *Fundamentals of Power Electronics*, New York, NY, USA: Springer, 2007.

[17] L. Zhang, L. Harnefors, and H. Nee, "Power-synchronization control of grid-connected voltage-source converters," *IEEE Trans. Power Syst.*, vol. 25, no. 2, pp. 809–820, May 2011.
[18] Z. Zhou, L. Zhang, Z. Liu, Q. Chen, R. Long, and H. Su, "Model predictive control for the receiving-side DC-DC converter of dynamic wireless power transfer," *IEEE Trans. Power Electron.*, vol. 35, no. 9, pp. 8985–8997, Sep. 2020.
[19] Y. Yang, W. Zhong, S. Kiratipongvoot, S. Tan, and S. Y. R. Hui, "Dynamic improvement of series–series compensated wireless power transfer systems using discrete sliding mode control," *IEEE Trans. Power Electron*, vol. 33, no. 7, pp. 6351–6360, Jul. 2018.
[20] K. Li, S. C. Tan, and R. Hui, "On beat frequency oscillation of two-stage wireless power receivers," *IEEE Trans. Power Electron.*, vol. 35, no. 12, pp. 12741–12751, Dec. 2020.
[21] J. Lee, and B. Han, "A bidirectional wireless power transfer EV charger using self-resonant PWM," *IEEE Trans. Power Electron.*, vol. 30, no. 4, pp. 1784–1787, Apr. 2015.
[22] K. Colak, E. Asa, M. Bojarski, D. Czarkowski, and O. C. Onar, "A novel phase-shift control of semibridgeless active rectifier for wireless power transfer," *IEEE Trans. Power Electron.*, vol. 30, no. 11, pp. 6288–6297, Nov. 2015.
[23] T. Diekhans, and R. W. De Doncker, "A dual-side controlled inductive power transfer system optimized for large coupling factor variations and partial load," *IEEE Trans. Power Electron.*, vol. 30, no. 11, pp. 6320–6328, Nov. 2015.
[24] M. Bennis, M. Debbah, and H. V. Poor, "Ultrareliable and low-latency wireless communication: Tail, risk, and scale," *Proc. IEEE*, vol. 106, no. 10, pp. 1834–1853, Oct. 2018.

Kerui Li (Student Member, IEEE) received the B.Eng. degree from the South China University of Technology, Guangzhou, China, in 2013, and the M.Eng. degree from the Sun Yat-sen University, Guangzhou, China, in 2016. He is currently working toward the Ph.D. degree with the Department of Electrical and Electronic Engineering, The University of Hong Kong, Hong Kong.

His research interests include topology, modeling, and control of power electronics converters and their applications to wireless power transfer systems.

Siew-Chong Tan (Senior Member, IEEE) received the B.Eng. (hons.) and M.Eng. degrees in electrical and computer engineering from the National University of Singapore, Singapore, in 2000 and 2002, respectively, and the Ph.D. degree in electronic and information engineering from the Hong Kong Polytechnic University, Hong Kong, in 2005.

He is currently a Professor with the Department of Electrical and Electronic Engineering, The University of Hong Kong, Hong Kong. He was a Visiting Scholar with Grainger Center for Electric Machinery and Electromechanics, University of Illinois at Urbana-Champaign, Champaign, IL, USA, from September to October 2009, and an Invited Academic Visitor of Huazhong University of Science and Technology, Wuhan, China, in December 2011. He is a co-author of the book Sliding Mode Control of Switching Power Converters: Techniques and Implementation (Boca Raton, FL, USA: CRC, 2011). His research interests include focused in the areas of power electronics and control, LED lightings, smart grids, and clean energy technologies.

Dr. Tan is currently an Associate Editor for the IEEE TRANSACTIONS ON POWER ELECTRONICS.

Shu Yuen Ron Hui (Fellow, IEEE) received the B.Sc. (hons.) degree in electrical and electronic engineering from the University of Birmingham, Birmingham, U.K., in 1984, and the D.I.C. and Ph.D. degrees from Imperial College London, London, U.K., in 1987.

He is concurrently the MediaTek Endowed Professor with the School of Electrical and Electronic Engineering, Nanyang Technological University, Singapore, and a part-time Chair Professor of power electronics with Imperial College London, London,U.K. He has published more than 300 refereed journal publications and book chapters, and more than 60 of his patents have been adopted by industry.

Dr. Hui is currently an Associate Editor for the IEEE TRANSACTIONS ON POWER ELECTRONICS and IEEE TRANSACTIONS ON INDUSTRIAL ELECTRONICS. He is an Editor of the IEEE JOURNAL OF EMERGING AND SELECTED TOPICS IN POWER ELECTRONICS. He is the recipient of the 2010 IEEE Rodulf Chope R&D Award, 2010 IET Crompton Medal, and 2015 IEEE William E. Newell Power Electronics Award. He is a fellow of the Australian Academy of Technological Sciences and Engineering, the US National Academy of Inventors, and also the Royal Academy of Engineering (U.K.).